Geophys. J. Int. (2007) **169,** 161–169 doi: 10.1111/j.1365-246X.2006.03276.x

Observations of long period Rayleigh wave ellipticity

Ana M. G. Ferreira and John H. Woodhouse

Department of Earth Sciences, University of Oxford, Parks Road, Oxford OX1 3PR, *UK. E-mail: Ana.Ferreira@earth.ox.ac.uk*

Accepted 2006 October 20. Received 2006 October 20; in original form 2006 July 18

SUMMARY

We analyse phase shifts and amplitude ratios of horizontal to vertical components of $T \sim 150$ s fundamental Rayleigh waves. In the ray picture of surface wave propagation, it is expected that at a single station this ratio will be constant, being controlled only by the seismic velocity structure beneath the seismic station. In contrast, we observe substantial variability in the amplitude ratios measured at a number of stations from the Global Seismic Network. We discuss possible causes for the anomalous ratios, concluding that they probably arise from effects associated with small scale heterogeneity distinctly distributed across different tectonic domains and having scale lengths shorter than a wavelength.

Key words: amplitude ratios, global seismic tomography, lateral heterogeneity, Rayleigh waves.

Downloaded from https://academic.oup.com/gji/article/169/1/161/648371 by guest on 22 July 2022

1 INTRODUCTION

For a smooth, laterally heterogeneous and transversely isotropic Earth, one can show that at a single station: (i) the phase shift between the horizontal and vertical components of fundamental Rayleigh waves is of 90° and (ii) the spectral ratio of horizontal to vertical fundamental Rayleigh waves is constant for all records, being determined by the local structure beneath the station (Woodhouse 1974; Tromp & Dahlen 1992a,b; Ferreira & Woodhouse 2007). This is the prediction of surface wave ray theory, which depends for its validity on the scale length of lateral heterogeneity being large compared with the wavelength.

Some studies of short period ($T = 10$–50 s) Rayleigh waves have exploited the latter property to determine the local crustal structure at the vicinity of a single recording station (Boore & Toksöz 1969; Sexton *et al.* 1977; Munirova & Yanovskaya 2001). These studies are based on surface wave ellipticity measurements, defined as the ratio of horizontal to vertical amplitudes, commonly referred to as H/V ratio, from three-component records at a single station. Several recent studies of ambient vibrations (typically between 0.1–10 Hz) also use H/V ratios to determine shallow, local S-wave velocity structure and for estimation of site-effects (e.g. Nakamura 1989; Fäh *et al.* 2003; Tanimoto & Alvizuri 2006). Since ambient vibrations are dominated by Rayleigh waves, the H/V ratio is assumed to measure their ellipticity, which depends on the local S-wave velocity structure.

In global seismology, most surface wave tomographic studies are based only on phase measurements, interpreted ray theoretically (e.g. Trampert & Woodhouse 1995, 1996; Ekström *et al.* 1997; van Heijst & Woodhouse 1999). In seeking further to refine these images, other types of data sensitive to smaller scale structure, such as polarization data and amplitudes, should become of greater importance. A number of global tomographic studies have incorporated polarization data (Laske *et al.* 1994; Laske & Masters 1996; Yoshizawa *et al.* 1999; Larson & Ekström 2002). However, the use of surface wave amplitudes in global tomography has been largely restricted to attenuation studies (for a review see e.g. Romanowicz & Durek 2000), for which there remains much scope for improvement.

In this study, we analyse amplitude ratios of horizontal to vertical components of long period, $T \sim 150$ s, fundamental Rayleigh waves recorded globally following large, shallow earthquakes. We shall refer to the amplitude ratios as HZ ratios, following the nomenclature of Tanimoto & Alvizuri (2006). We discuss possible causes for the observed variability of the amplitude ratios at each station. Furthermore, we compare the HZ ratios measured from data with those from synthetics calculated using the Spectral Element Method (SEM) as implemented by Komatitsch & Tromp (2002a,b) to further interpret the observed variability of amplitude ratios.

2 THEORETICAL BACKGROUND

Woodhouse (1974) introduced the concept of local modes, showing that, asymptotically, the local eigenfunctions at each point $\hat{\mathbf{r}}$ are identical to those that determine the surface wave eigenfunctions on a spherically symmetric Earth whose properties are everywhere equal to those beneath $\hat{\mathbf{r}}$. Thus, the predicted HZ ratio can be calculated, for a given local model, using a standard surface wave or normal mode algorithm (e.g. Woodhouse 1988). Calculations using the spherically symmetric Earth model PREM (Dziewonski & Anderson 1981) give a value of *HZ ratio* $= 0.78$ for $T = 150$ s Rayleigh waves. We shall refer to this calculated value as the *PREM prediction*. We also carry out calculations using the global crust model CRUST2.0 (Bassin *et al.* 2000) combined with mantle model S20RTS (Ritsema *et al.* 1999). We shall refer to these predictions as *3-D local mode predictions*. The top diagram in Fig. 6 shows the global distribution of 3-D local mode predicted ratios for $T =$ 150 s Rayleigh waves. Globally, the maximum variation of 3-D

© 2007 The Authors
Journal compilation © 2007 RAS

local mode predictions is of 29 per cent, but if we restrict ourselves to continents, where most of seismic stations from global networks are located, the maximum variation of predicted ratios reduces to 17 per cent.

3 MEASURING HZ AMPLITUDE RATIOS AND PHASE SHIFTS

3.1 Data selection and processing

The data which are used in this study are long period, minor-arc three-component surface wave seismograms from the Global Seismic Network (GSN) with high signal-to-noise ratio. We are interested in fundamental-mode Rayleigh waves, so our data set satisfies several criteria to reduce contamination from S waves and higher modes. The earthquakes are shallow (depth $\leq$50 km), to minimize overtone contamination, and large enough to excite low-noise long period mantle waves ($M_{\rm w} > 6.5$). We consider only source–receiver pairs whose minor-arc distance lies in the range $50^\circ \leq \Delta \leq 120^\circ$, to avoid near-source effects, caustics and multiple orbit overlapping wave trains. In order to avoid interference from multiple simultaneous arrivals, we discard source–receiver pairs for which multipathing is predicted to occur. We perform a systematic detection of multipathing using the algorithm described by Ferreira & Woodhouse (2007), Ferreira (2005) and Tape (2003) applied to the global phase velocity maps of Trampert & Woodhouse (1995, 1996) and of van Heijst & Woodhouse (1999) for fundamental Rayleigh waves with period $T = 150$ s. We also exclude Rayleigh waves at source–receiver azimuths close to nodes of the fundamental mode source amplitude radiation pattern, as they are likely to be dominated by scattered energy. For each earthquake we calculate the amplitude radiation pattern of $T = 150$ s Rayleigh waves as described in Ferreira & Woodhouse (2006). We exclude source–receiver pairs at azimuths for which the amplitude is smaller than half of the maximum amplitude of the calculated radiation pattern.

Instrument response deconvolution is conducted on the seismograms and the horizontal components are rotated into longitudinal and transverse directions for each earthquake. All the seismograms are filtered using a Gaussian bandpass filter centred around $T = 150$ s with a width of 1200 s. A time window is selected centred on the maximum amplitude of the desired wavetrain, with its edges at zero-crossings of the seismograms, to minimize errors in the measurements.

We have carried out the data selection and processing using records from stations of the GSN for 42 earthquakes well distributed globally. In this paper, we shall illustrate our results for seven stations: WMQ, FFC, GUMO, KIP, HRV, PAS and PFO.

3.2 Measurements

We carry out measurements of both phase shifts and amplitude ratios of horizontal to vertical components of Rayleigh waves in the time domain. In order to align the vertical and horizontal component records, we apply a Hilbert transform to the horizontal component Rayleigh waves and compare them with the negative of the vertical component records. We use two methods to measure HZ ratios and phase shifts:

3.2.1 Method I

The phase shift is calculated by cross-correlation between the vertical and horizontal component records. The amplitude ratio HZ is approximated by $HZ\,ratio \approx \sqrt{\frac{P_H}{P_Z}}$, where P_Z is the power in the vertical component record and P_H is the power in the horizontal component record. The power is obtained through the sum of the squared amplitude within the selected time window.

3.2.2 Method II

A non-linear least-squares algorithm calculates the phase shift and amplitude factor that best fits the negative of the vertical component seismogram within the selected time window to the Hilbert transform of the horizontal component seismogram.

Fig. 1 shows measurements of HZ ratios and phase shifts between the horizontal and vertical components of Rayleigh waves from mode summation synthetic seismograms using PREM for the source–receiver pairs selected for the seven illustrative stations used in this paper. The seismograms are calculated summing a large number of overtones. The measured amplitude ratios and phase shifts are quite stable. The maximum deviation of the measured HZ ratios is of

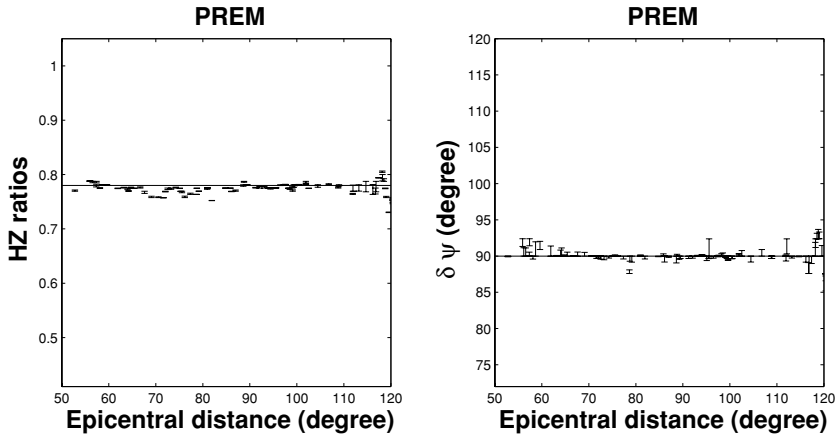

Figure 1. HZ ratios and phase shifts of $T \sim 150$ s Rayleigh waves from mode summation synthetic seismograms using PREM. The synthetics are calculated summing a large number of overtones. The measurements are carried out at seven different stations from the GSN, following 42 large, shallow earthquakes. We present two measurements, connected by a vertical line, which are carried out using the two different methods described in Section 3.2. The horizontal solid lines are PREM predictions for fundamental $T \sim 150$ s Rayleigh waves. All the measurements are shown as a function of increasing source–receiver epicentral distance.

Downloaded from https://academic.oup.com/gji/article/169/1/161/648371 by guest on 22 July 2022

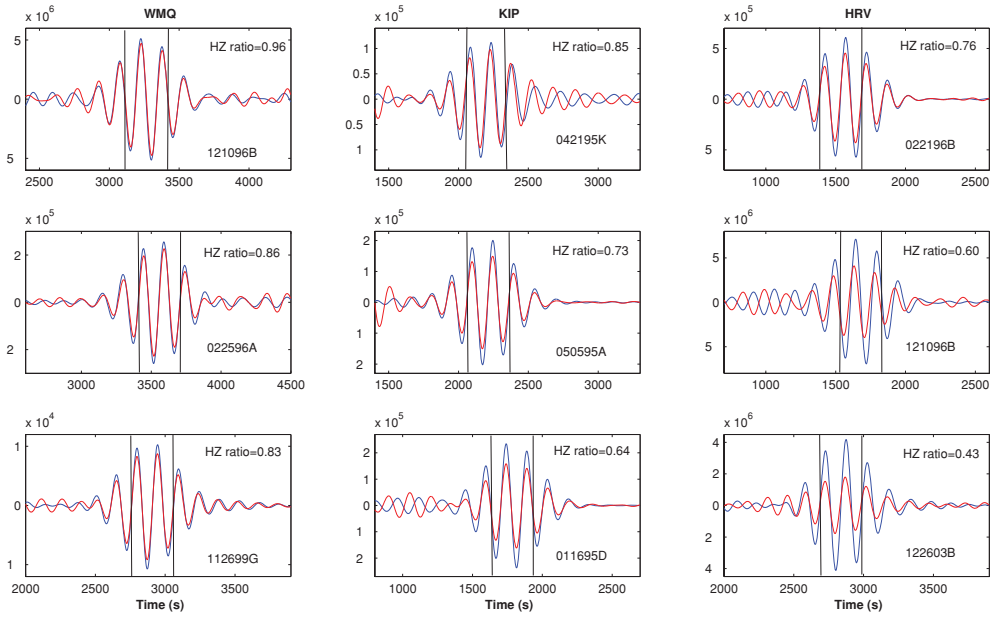

Figure 2. Comparison of vertical (blue) and horizontal (red) components of long period ($T \sim 150$ s) Rayleigh wave records at GSN stations WMQ, KIP and HRV, following several earthquakes. The horizontal component records have been Hilbert transformed, being compared with the negative of the vertical component record. The vertical lines (black) indicate the selected time windows. The CMT code corresponding to each earthquake is shown in the bottom right corner of each diagram. The measured HZ ratios are also shown, which are calculated using method I, described in Section 3.2. Local mode predictions using crust model CRUST2.0 and mantle model S20RTS are *HZ ratio* = 0.87 for station WMQ, *HZ ratio* = 0.76 for station KIP and *HZ ratio* = 0.84 for station HRV.

9 per cent from the PREM prediction and the measured phase shifts have a maximum deviation of 3.7° from 90°; these deviations reflect errors in the measurements induced by overtone contamination.

3.3 Results

Fig. 2 shows comparisons of vertical component (blue) seismograms with horizontal component (red) seismograms recorded at three different stations, following various earthquakes. All the traces are bandpass filtered around $T \sim 150$ s. We also show the selected time window for each trace. For station WMQ, the ratios are relatively stable. There is considerable variability of the HZ ratios at stations KIP and HRV. Furthermore, there is appreciable variation of the HZ ratios from station to station. For $T = 150$ s, local mode predictions provide the ratios *HZ ratio* = 0.87 for station WMQ, *HZ ratio* = 0.76 for station KIP and *HZ ratio* = 0.84 for station HRV. It is clear that whereas for station WMQ the local mode prediction is close to the measured ratios shown in Fig. 2, for stations KIP and HRV the deviations are larger.

Figs 3–5 show HZ ratios and phase shifts measured using the two methods described in Section 3.2 for various earthquakes recorded at the seven GSN stations used in this study. Fig. 3 shows measurements for stations WMQ and FFC, which are located within the interior of the Asian and North American continents, respectively. Fig. 4 shows measurements for stations KIP and GUMO, which are located in ocean islands (in Hawaii and in the Marianas islands, respectively). Finally, Fig. 5 shows results for stations HRV, PAS and PFO, which are located near the eastern and western North American continental margins, respectively. PAS and PFO are nearby stations, 169 km apart.

The measured HZ ratios at station WMQ have moderate variability, with the greatest deviation between the maximum and minimum measured values being 17.6 per cent. The measured phase shifts lie in the range 80°–92°, which is close to the expected value of $\delta\psi = 90°$. For station FFC there is larger variability in the measured HZ ratios, with the greatest deviation being 27 per cent. The measured phase shifts lie in the range 85°–95°.

At the ocean island stations KIP and GUMO, there is moderate variability in the measured ratios, with the greatest deviation being 20 per cent for KIP and 19 per cent for GUMO. The ranges of measured phase shifts are larger than for the continental stations WMQ and FFC, being 80°–104° for station KIP and 72°–94° for station GUMO.

HZ ratio and phase shift measurements at near continental margin stations HRV, PAS and PFO show considerable variability. The largest deviation in the measured HZ ratios at stations PAS, PFO and HRV is of 20, 31 and 42 per cent, respectively. The corresponding phase shifts are 81°–107°, 82°–99° and 84°–120°.

Measurements for nearby earthquakes recorded at the same station are generally consistent (e.g. for the earthquake pair 11–12 recorded at WMQ; for earthquake pair 12–13 at KIP; for earthquake pairs 3–4 at GUMO; for earthquake pair 5–6 at HRV; for earthquake pairs 1–3 and 7–8 at PAS). However, occasionally the ratios and phase shifts at a single station vary significantly even for closely spaced earthquakes. For example, at station FFC the amplitude ratios for the earthquake pair 10–11 are *HZ ratio* = 0.73 and *HZ ratio* = 0.84, respectively. These earthquakes occurred within fourteen days of one another, which gives us confidence that instrumental response has not changed over the recording time interval. The Rayleigh wave paths connecting these earthquakes to FFC are very similar. This suggests that near-source finite frequency effects due to small scale heterogeneity may be responsible for these variations. van der Lee (1998) also identified amplitude anomalies of fundamental Rayleigh waves probably related to near-source Earth structure. Similarly, at station KIP, the ratios for the same

Downloaded from https://academic.oup.com/gji/article/169/1/161/643371 by guest on 22 July 2022

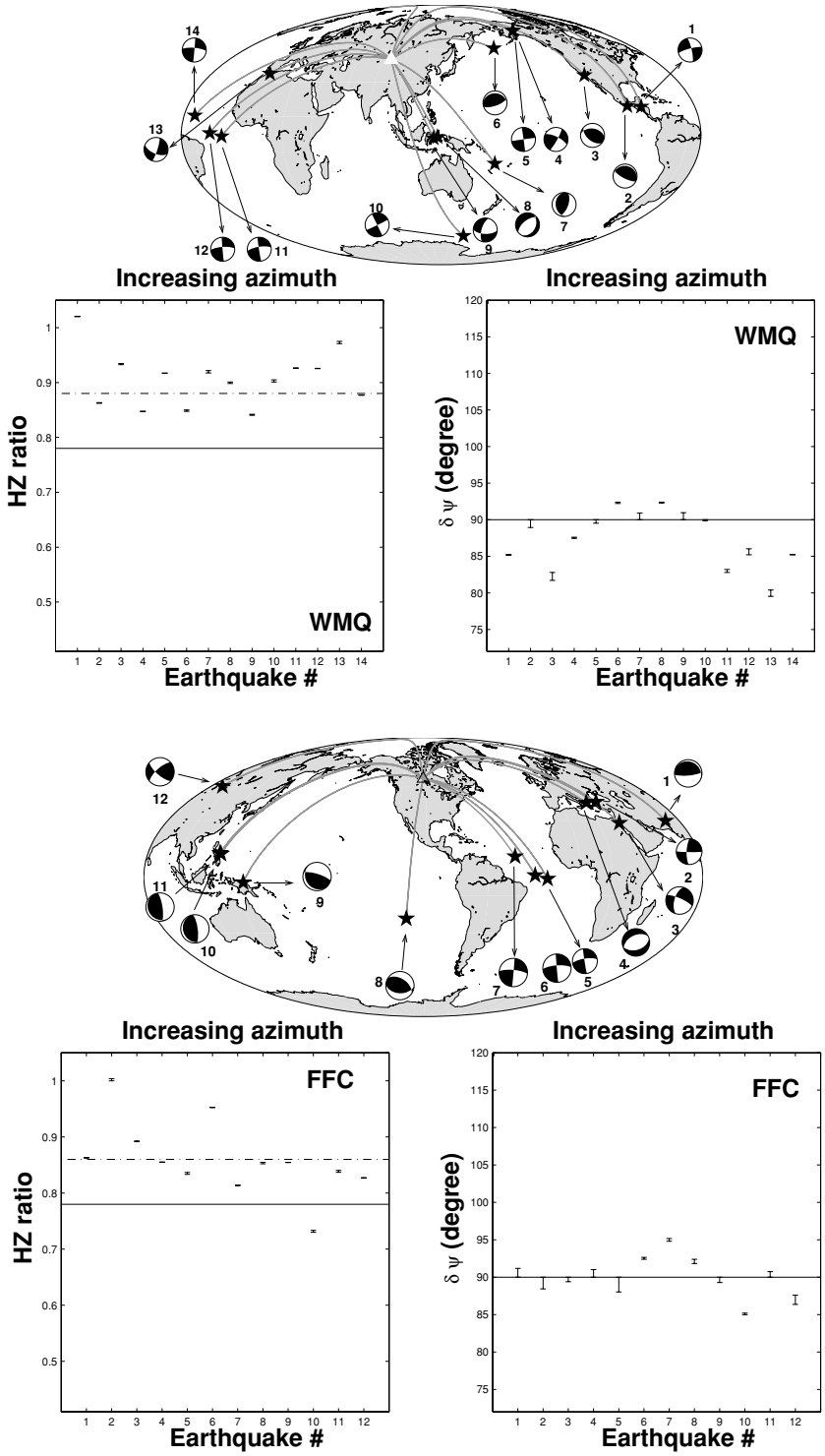

Figure 3. HZ ratios and phase shifts of $T \sim 150$ s Rayleigh waves measured at the continental stations WMQ and FFC, for the earthquakes with Harvard CMT centroid locations and focal mechanisms shown at the top diagrams. We present two measurements, connected by a vertical line, which are carried out using the two different methods described in Section 3.2. The horizontal solid lines are PREM predictions, whereas the horizontal dot-dashed lines are 3-D local mode predictions. All the measurements are presented as a function of increasing azimuth at the station. Note that the azimuth axis scale is not linear.

earthquakes (earthquakes 9 and 10 in Fig. 4) are *HZ ratio* = 0.85 and *HZ ratio* = 0.74, respectively. The same type of features are found for earthquakes 7 and 8 at station HRV and the same earthquakes at station FFC (which correspond to earthquakes 5 and 6 in Fig. 3).

Examining the two nearby stations at California, PAS and PFO, it is interesting that for some earthquakes there is a considerable difference in the ratios at the two stations. For example, for earthquake 1, at station PAS the HZ *ratio* is *HZ ratio* = 0.82, whereas at PFO the ratio is *HZ ratio* = 0.96. Since the Rayleigh waves travelling from

Downloaded from https://academic.oup.com/gji/article/169/1/161/648371 by guest on 22 July 2022

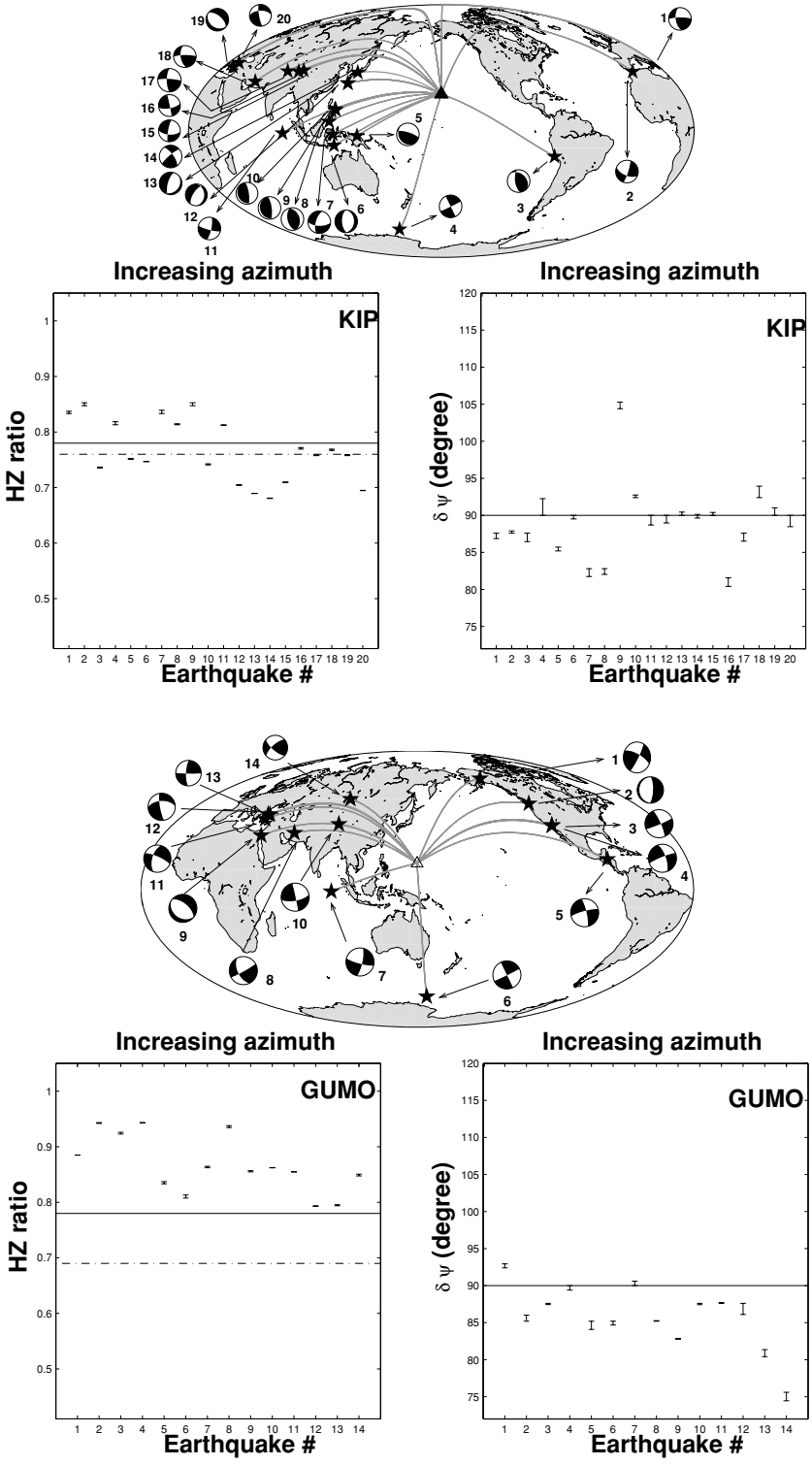

Figure 4. Same as in Fig. 3, but for the oceanic stations KIP and GUMO for the earthquakes with Harvard CMT centroid locations and focal mechanisms shown at the top diagrams.

the earthquake source to the two stations follow very similar paths, this suggests that small scale heterogeneity effects near the receiver are the cause of the differences. A number of studies of surface wave polarization have also reported anomalous waveforms due to various mechanisms taking place near the receiver (e.g. Paulssen *et al.* 1990; Levshin *et al.* 1992, 1994).

Comparing the observed ratios with predictions, for station WMQ, the PREM prediction underestimates the measured HZ ratios, whereas the local mode prediction lies within the range of observed ratios, being close to its average, which is 0.90. The same happens for station FFC. For station GUMO, both predictions underestimate the measured ratios, with the PREM prediction being

© 2007 The Authors, *GJI*, **169,** 161–169
Journal compilation © 2007 RAS

Downloaded from https://academic.oup.com/gji/article/169/1/161/648371 by guest on 22 July 2022

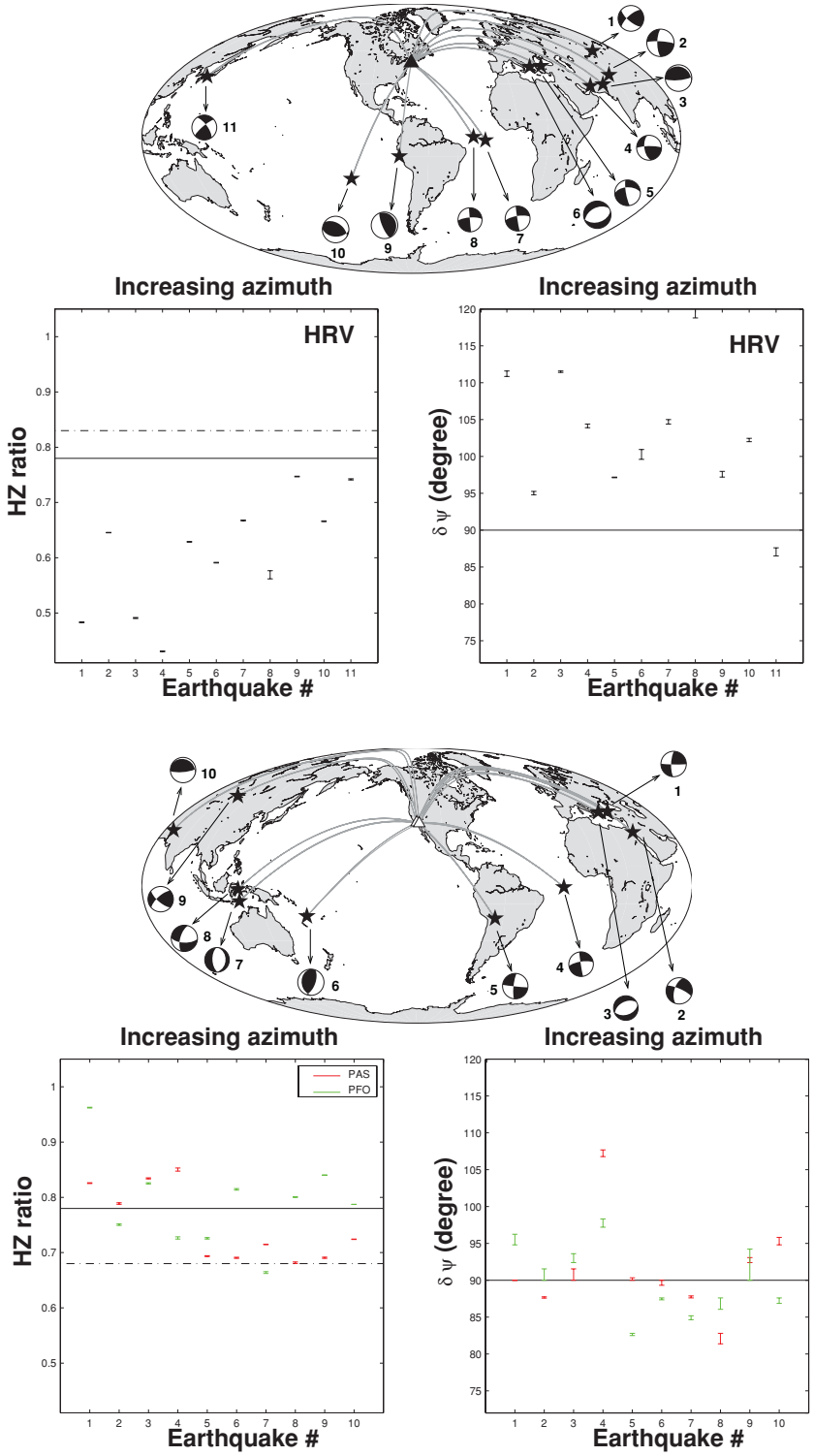

Figure 5. Same as in Fig. 3, but for the continental margin stations HRV, PAS and PFO, for the earthquakes with Harvard CMT centroid locations and focal mechanisms shown at the top diagrams.

closer to the measurements, whereas for station HRV both predictions overestimate the ratios. For the other stations, both predictions lie within the large range of measured ratios.

For some stations the measured HZ ratios suggest some dependence on receiver-source azimuth. For example, the overall pattern of HZ ratios at stations FFC and GUMO seems to decrease with azimuth, whereas for station HRV the pattern of HZ ratios seems to increase with azimuth. This suggests that the measured ratios may be influenced by finite frequency effects along the path or by azimuthal anisotropy.

We have also examined the measured amplitude ratios and phase shifts shown in Figs 3–5 not only as a function of station-source azimuth, but also as a function of source–receiver epicentral distance, as a function of time of the record and as a function of the

Downloaded from https://academic.oup.com/gji/article/169/1/161/648371 by guest on 22 July 2022

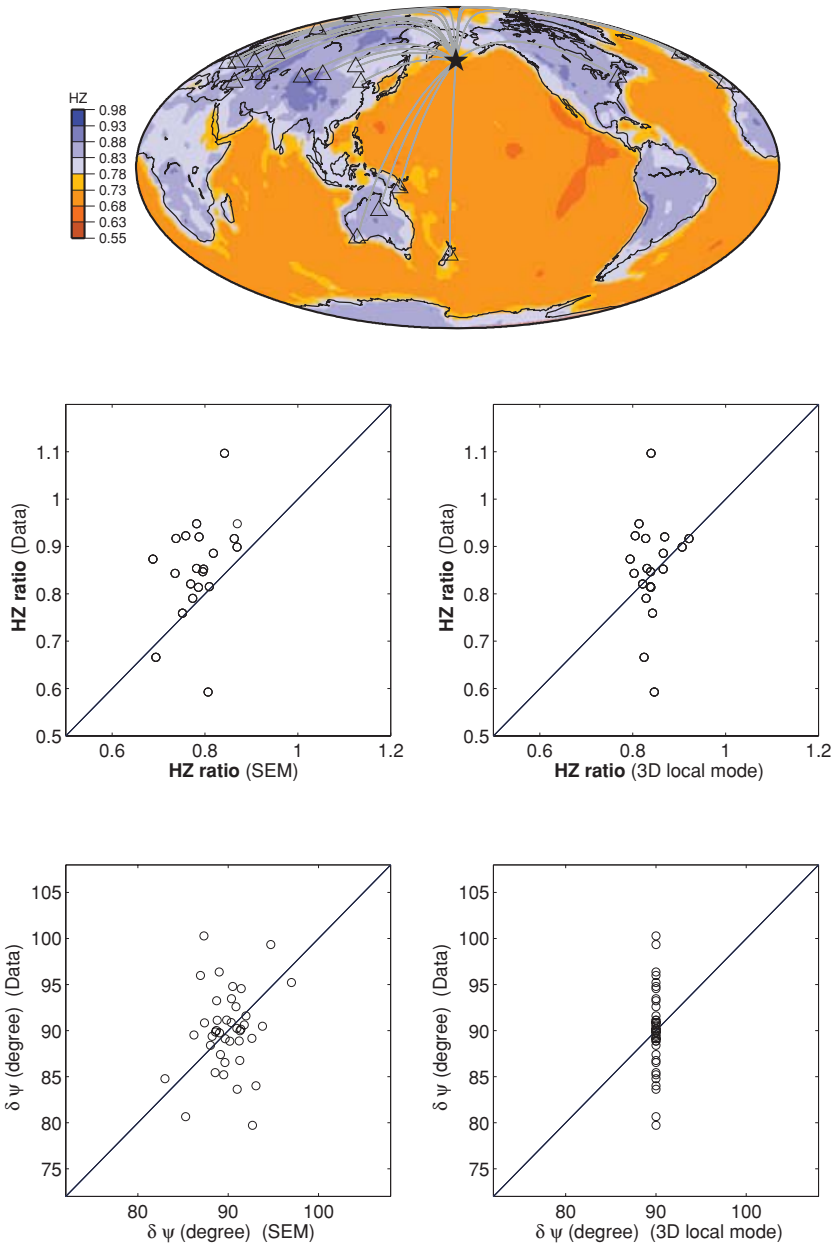

Figure 6. Comparison between observed and predicted $T \sim 150$ s HZ ratios and phase shifts for the $M_w = 6.7$ earthquake in Rat Islands on 1996 March 14, recorded at various stations. (Top) Great circle paths connecting the source (star) and the considered stations (triangles) superimposed on the global distribution of 3-D local mode predictions of HZ ratios for $T = 150$ s Rayleigh waves. (Bottom) Measurements on data (Data) are compared with those from Spectral Element Method synthetics (SEM) and with 3-D local mode predictions.

distance of the station to a node in the source amplitude radiation pattern. We did not find a significant relationship between our measurements and these parameters. Furthermore, we have carried out measurements at other periods ($T = 100$, 80 and 50 s) and we also observe substantial variability in the amplitude ratios. In order to study the frequency dependency of the observations for shorter periods, it would be more suitable to carry out measurements in the frequency domain. This will be the subject of future work.

4 DISCUSSION

In the previous section, we identified finite frequency effects by small scale heterogeneity as a possible reason for the moderate to large range of phase shifts and HZ ratios of Rayleigh waves measured at the GSN stations used in this paper. When lateral variations in Earth structure are sharp, occurring at scale lengths smaller than the wavelengths in the wavefield, various complications in wave propagation may arise, such as coupling of Rayleigh waves with Love waves and interference with scattered waves. As we selected the data in order to minimize the amplitudes of overtones and multipathing effects, we discard overtone contamination and multipathing as the main causes for the anomalous observations. Lateral heterogeneity also causes ray bending, which affects the measured ratios. Nevertheless, for $T \sim 150$ s the maximum reported arrival angle deviation is of 15° (Laske 1995), which would cause a variation in the amplitude ratios of 4 per cent, which is much smaller than the

Downloaded from https://academic.oup.com/gji/article/169/1/161/648371 by guest on 22 July 2022

variations we observe. Also, there are no reports of significant incorrect alignment of the horizontal components of the seismometers in the stations we use (Laske 1995; Larson & Ekström 2002). Anisotropy can also affect the HZ ratios and hence it is a candidate to explain at least part of the observed variability. This issue goes beyond the scope of this paper and deserves further investigation.

To further interpret our observations, we calculate HZ amplitude ratios and phase shifts between horizontal and vertical components of synthetic seismograms calculated using the Spectral Element Method (SEM). This method is an accurate, purely numerical technique for the full calculation of the seismic wavefield in realistic 3-D models (for a review see e.g. Chaljub *et al.* 2006; Komatitsch *et al.* 2005). We use the crustal model CRUST2.0 and mantle model S20RTS to describe *S*-wave velocity variations in the mantle (V_s). The *P*-wave velocity in the mantle, V_p, is assumed to be related to V_s through a depth-dependent scaling factor $R = d \ln V_s / d \ln V_p$, which increases linearly from 1.3 at the surface to 3.0 at the core–mantle boundary (Ritsema & van Heijst 2002). Fig. 6 compares measured amplitude ratios and phase shifts from real data seismograms with SEM predictions for the 1996 March 14, $M_w = 6.7$ earthquake in Rat Islands, Alaska recorded at the 20 stations shown in the top diagram. All the measurements are made using method I, as described in Section 3.2. For reference, we also show plots comparing data with 3-D local mode predictions. The 3-D local mode predictions have a much narrower range of amplitude ratios than those measured in the data, with very little correlation between predictions and observations. SEM predictions match the character of the data better than do 3-D local mode predictions. Nevertheless, overall the variation in HZ ratios is still somewhat underpredicted. The observed discrepancies must be due to to inaccuracies inherent with the SEM and, most importantly, to uncertainties in the Earth model. Indeed, as is the case for most current global *S*-wave velocity models, S20RTS is a very smooth model, with a resolution of about 1000 km at the Earth's surface (see Romanowicz 2003, for a review and comparison of recent mantle models). The results of our analysis suggest that the observed variability of amplitude ratios and phase shifts may be due to finite frequency effects by small scale heterogeneity, which is not yet resolved by current global tomographic models. Potentially, the amplitude ratios of long period Rayleigh waves provide independent information about the deep structure of the Earth, which could be combined with other types of measurements (e.g. phase measurements) to reduce the non-uniqueness of Earth models and to determine local shear wave velocity structure from a single station. Nevertheless, this study suggests that care should be taken when interpreting long period HZ ratios as being uniquely controlled by local structure beneath the recording station. Furthermore, the variety of observations in different tectonic environments — oceanic islands, continental margins and continental interiors — suggests that heterogeneity may be distributed differently across such environments.

5 CONCLUSIONS

In this paper, we investigate phase shifts and amplitude ratios of the horizontal to vertical components of $T \sim 150$ s fundamental Rayleigh waves recorded at seven illustrative stations from the GSN. We observe a moderate to large variability of amplitude ratios, in contrast to what is expected for a smooth laterally varying Earth. The analysis of these anomalies as a function of azimuth and for waves with similar paths, together with the comparison with synthetic seismograms calculated using the Spectral Element Method for a 3-D Earth model suggest that the most likely cause for the anomalous observations are finite frequency effects due to small scale heterogeneity that is not yet imaged by current global tomographic Earth models. Furthermore, this study suggests that care should be taken when interpreting long period HZ ratios as being uniquely controlled by the local structure beneath the recording station.

ACKNOWLEDGMENTS

AMGF is supported by a NERC postdoctoral fellowship under grant NE/C510916/1. We gratefully acknowledge the availability of global seismograms from the IRIS/IDA/USGS networks and the IRIS Data Centre. Data and computing facilities at Oxford have been supported under NERC grants NER/F/S/2001/00369 and NE/B505997/1. We are grateful to D. Komatitsch and J. Tromp for freely distributing their SEM code.

REFERENCES

Bassin, C., Laske, G. & Masters, G., 2000. The current limits of resolution for surface wave tomography in North America, *EOS, Trans. Am. geophys. Un.,* **F897,** 81.

Boore, D.M. & Toksöz, M.N., 1969. Rayleigh wave particle motion and crustal structure, *Bull. seism. Soc. Am.,* **59,** 331–346.

Chaljub, E., Komatitsch, D., Vilotte, J.-P., Capdeville, Y., Valette, B. & Festa, G., 2006. Spectral element analysis in seismology, in *Advances in Wave Propagation in Heterogeneous Media (Advances in Geophysics series)*, eds Wu, R.-S. & Maupin, V., Elsevier, San Diego.

Dziewonski, A.M. & Anderson, D., 1981. Preliminary Reference Earth Model, *Phys. Earth planet. Inter.,* **25,** 297–356.

Ekström, G., Tromp, J. & Larson, E.W.F., 1997. Measurements and global models of surface wave propagation, *J. geophys. Res.,* **102,** 8137–8157.

Fäh, D., Kind, F. & Giardini, D., 2003. Inversion of local S-wave velocity structures from average H/V ratios, and their use for the estimation of site-effects, *J. Seismol.,* **7**(4), 449–467.

Ferreira, A.M.G., 2005. Seismic Surface Waves in the Laterally Heterogeneous Earth, *DPhil thesis,* University of Oxford.

Ferreira, A.M.G. & Woodhouse, J., 2006. Long period seismic source inversions using global tomographic models, *Geophys. J. Int.,* **166**(3), 1178–1192.

Ferreira, A.M.G. & Woodhouse, J. H., 2007. Source, path and receiver effects on seismic surface waves, *Geophys. J. Int.,* **168,** 109–132.

Komatitsch, D. & Tromp, J., 2002a. Spectral-element simulations of global seismic wave propagation—I. Validation, *Geophys. J. Int.,* **149,** 390–412.

Komatitsch, D. & Tromp, J., 2002b. Spectral-element simulations of global seismic wave propagation—II. Three-dimensional models, oceans, rotation and self-gravitation, *Geophys. J. Int.,* **150,** 308–318.

Komatitsch, D., Tsuboi, S. & Tromp, J., 2005. The spectral-element in seismology, in *Seismic Earth: Array analysis of Broadband seismograms*, Vol. 157, pp. 205–228, eds Levander, A. & Nolet, G., Geophysical Monograph AGU.

Larson, E.W.F. & Ekström, G., 2002. Determining surface wave arrival angle anomalies, *J. geophys. Res.,* **107,** 2127.

Laske, G., 1995. Global observation of off-great-circle propagation of long period surface waves, *Geophys. J. Int.,* **123,** 245–259.

Laske, G. & Masters, G., 1996. Constraints on global phase velocity maps from long-period polarization data, *J. geophys. Res.,* **101,** 16 059–16 075.

Laske, G., Masters, G. & Zürn, W., 1994. Frequency-dependent polarization measurements of long-period surface waves and their implications for global phase velocity maps, *Phys. Earth planet. Inter.,* **84,** 111–137.

Levshin, A.L., Ratnikova, L. & Berger, J., 1992. Peculiarities of surface-wave propagation across central Eurasia, *Bull. seism. Soc. Am.,* **82**(6), 2464–2493.

Levshin, A.L., Ritzwoller, M. & Ratnikova, L., 1994. The nature and cause of polarization anomalies of surface waves crossing northern and central Eurasia, *Geophys. J. Int.,* **117,** 577–590.

Downloaded from https://academic.oup.com/gji/article/169/1/161/648371 by guest on 22 July 2022

Munirova, L.M. & Yanovskaya, T.B., 2001. Spectral ratio of the horizontal and vertical Rayleigh wave components and its application to some problems of seismology, *Izvestiya, Phys. Solid Earth,* **37**(9), 10–18.

Nakamura, Y., 1989. A method for dynamic characteristics estimation of subsurface using microtremor on the ground surface, *QR Railway Tech. Res. Inst.,* **20,** 1.

Paulssen, H., Levshin, A.L., Lander, A.V. & Snieder, R., 1990. Time-dependent and frequency-dependent polarization analysis—anomalous surface-wave observations in Iberia, *Geophys. J. Int.,* **103,** 483–496.

Ritsema, J. & van Heijst, H., 2002. New constraints on the P velocity structure of the mantle from P, PP, PPP, and PKPab travel-times, *Geophys. J. Int.,* **149,** 482–489.

Ritsema, J., van Heijst, H. & Woodhouse, J., 1999. Complex shear wave velocity structure imaged beneath Africa and Iceland, *Science,* **286,** 1925–1928.

Romanowicz, B., 2003. Global mantle tomography: Progress status, *Annu. Rev. Earth Planet. Sci.,* **31,** 303–328.

Romanowicz, B. & Durek, J., 2000. Attenuation in the earth: a review, in *Earth's Deep Interior: Mineral Physics and Tomography from the Atomic to the Global Scale*, Vol. 117, pp. 161–180, eds Karato, S., Forte, A.M., Liebermann, R.C., Masters, G. & Stixrude, L., Geophysical Monograph AGU.

Sexton, J.L., Rudman, A.J. & Mead, J., 1977. Ellipticity of Rayleigh waves recorded in the Midwest, *Bull. seism. Soc. Am.,* **67**(2), 369–382.

Tanimoto, T. & Alvizuri, C., 2006. Inversion of the HZ ratio of microseisms for S-wave velocity in the crust, *Geophys. J. Int.,* **165**(1), 323–335.

Tape, C.H., 2003. Waves on a Spherical Membrane, *MSc thesis,* University of Oxford.

Trampert, J. & Woodhouse, J.H., 1995. Global phase-velocity maps of Love and Rayleigh-waves between 40 and 150 seconds, *Geophys. J. Int.,* **122,** 675–690.

Trampert, J. & Woodhouse, J.H., 1996. High resolution global phase velocity distributions, *Geophys. Res. Lett.,* **23,** 21–24.

Tromp, J. & Dahlen, F.A., 1992a. Variational principles for surface wave propagation on a laterally heterogeneous earth—I. Time-domain JWKB theory, *Geophys. J. Int.,* **109,** 581–598.

Tromp, J. & Dahlen, F.A., 1992b. Variational principles for surface wave propagation on a laterally heterogeneous earth—II. Frequency-domain JWKB theory, *Geophys. J. Int.,* **109,** 599–619.

van der Lee, S., 1998. Observations and origin of Rayleigh-wave amplitude anomalies, *Geophys. J. Int.,* **135,** 691–699.

van Heijst, H.J. & Woodhouse, J.H., 1999. Global high-resolution phase velocity distributions of overtone and fundamental-mode surface waves determined by mode branch stripping, *Geophys. J. Int.,* **137,** 601–620.

Woodhouse, J.H., 1974. Surface waves in a laterally varying layered structure, *Geophys. J. R. astr. Soc.,* **37,** 461–490.

Woodhouse, J.H., 1988. The calculation of the eigenfrequencies and eigenfunctions of the free oscillations of the earth and the sun, in *Seismological Algorithms*, pp. 321–370, ed. Doornbos, D.J., Academic Press, San Diego.

Yoshizawa, K., Yomogida, K. & Tsuboi, S., 1999. Resolving power of surface wave polarization for higher-order heterogeneities, *Geophys. J. Int.,* **138,** 205–220.

Downloaded from https://academic.oup.com/gji/article/169/1/161/648371 by guest on 22 July 2022